Close-to-conformal versus Hertz superposition: a comparison for two-dimensional contact

Lucas da Silva[1], Alfredo Gay Neto[1]

[1]*Dept. of Structural and Geotechnical Engineering, Polytechnic School at the University of São Paulo*
Av. Prof. Luciano Gualberto, 380 – Butantã, 05508-010, São Paulo, Brazil
lucas7.silva@usp.br, alfredo.gay@usp.br

Abstract. The purpose of this research is to investigate the limitations of the Hertz contact model for pointwise contact in scenarios with nearby contact points. Many dynamic applications utilize this force model for pointwise contact between solid particles. However, the theory assumes non-conformal contact. Consequently, its application to concave geometries, which may involve multiple contact points and conformality, can lead to inaccuracies. We examine the planar contact between a convex particle and a concavity in two configurations, each with two contact points. In the first, the points are widely separated, resulting in isolated contact patches. In the second, referred to as "close-to-conformal," the points are close enough to affect one another. Using a deformable finite element model, we obtain the pressure distributions generated by pressing the convex particle against the concavity and compare them with predictions of Hertz theory. Our results show that the pressure deviates from the expected semi-elliptical shape depending on the loading. The close-to-conformal configuration, in particular, produces non-Hertzian pressures even under small loads. This demonstrates that accurately representing the elasticity of the bodies requires an alternative force model for pointwise contact.

Keywords: two-dimensional contact, conformal contact, Hertz contact theory.

1 Introduction

The contact framework presented in [1] has a contact enforcement method using a hybrid interface law comprised of a barrier part and a physical-based part. It is possible to model the hertz force law with adequate parameters [2]. The Hertz force law is restricted to non-conformal contact. The non-conformal contact hypothesis raises little concern in the contact between convex bodies, however, in the presence of a concavity, one must pay attention to the possibility of multiple contact points existing and interfering with each other.

As seen in [3], the Hertz solution can be achieved considering quadratic approximations of the contact surfaces about the contact point. In this quadratic model, the surfaces are locally identical when their curvatures match, which can be seen as a conformal contact. For convex-concave contact, there may be configurations with two near plausible contact pairs and a non-plausible contact pair in between. Although the non-plausible contact pair is a local maximizer of distance an intense enough load can close this gap, and, consequently, the whole segment between the plausible contact pairs would come into contact, and there would be a single contact patch for supposedly two contact points, a clear indication of conformal contact. A practical manifestation of this fact appears in wheel-rail contact, Magel and Kalousek [4] define it as conformal if the measurement of the gap in the region between two points of contact is below a predefined value.

The goal of this work is to investigate the applicability of Hertz theory in this situation, and if it is possible to consider the supposedly independent contact pairs as Hertzian and sum their effects to find the pressure distribution or if the mutual interference requires a more refined theory.

2 Convex-concave contact pairs in the master-master approach

Gay Neto and Wriggers [5] consider pointwise contact interactions addressed by the master-master formulation. In this approach, for each pair of parametrized contact surfaces $\Gamma_A(\zeta_A, \theta_A)$ and $\Gamma_B(\zeta_B, \theta_B)$, the coordinates of a pair of points that are prone to contact or effectively in contact are defined as the solution of the four orthogonality relations, referred to as the local contact problem (LCP),

$$\begin{aligned}(\Gamma_A - \Gamma_B) \cdot \frac{\partial \Gamma_A}{\partial \zeta_A} &= 0\\ (\Gamma_A - \Gamma_B) \cdot \frac{\partial \Gamma_A}{\partial \theta_A} &= 0\\ -(\Gamma_A - \Gamma_B) \cdot \frac{\partial \Gamma_B}{\partial \zeta_B} &= 0\\ -(\Gamma_A - \Gamma_B) \cdot \frac{\partial \Gamma_B}{\partial \theta_B} &= 0\end{aligned} \quad . \tag{1}$$

A solution of eq. (1) has the property that the gap vector $\mathbf{g} = \Gamma_A(\bar{\zeta}_A, \bar{\theta}_A) - \Gamma_B(\bar{\zeta}_B, \bar{\theta}_B)$ is orthogonal to the four coordinates lines passing through $\Gamma_A(\bar{\zeta}_A, \bar{\theta}_A)$ and $\Gamma_B(\bar{\zeta}_B, \bar{\theta}_B)$, hence orthogonal to the tangent planes at these points.

In two dimensions, the boundaries become parametrized planar curves $\Gamma_A(\zeta)$ and $\Gamma_B(\theta)$, and there are two orthogonality relations

$$\begin{aligned}(\Gamma_A - \Gamma_B) \cdot \frac{\partial \Gamma_A}{\partial \zeta} &= 0\\ -(\Gamma_A - \Gamma_B) \cdot \frac{\partial \Gamma_B}{\partial \theta} &= 0\end{aligned} \quad . \tag{2}$$

Geometrically, the gap vector is orthogonal to both curves at the solution points as indicated in Fig. 1. The gap vector defines a common normal line to both curves.

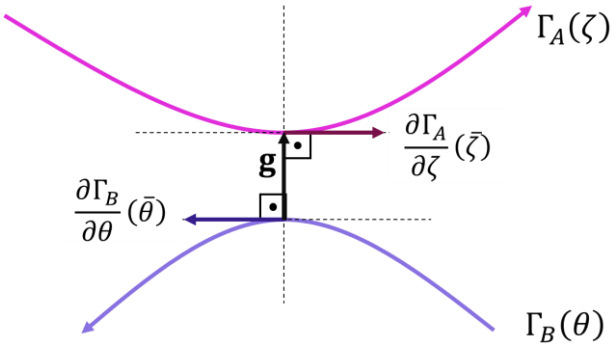

Figure 1. Contact boundaries and the LCP solution

In a non-convex contact, multiple solutions of eq. (1) or eq. (2) may exist while not all of them should be considered as contact candidates. Gay Neto and Wriggers [5] define a solution of the LCP as non-plausible as a contact candidate when contact must take place elsewhere. For instance, in Fig. 2(a), the red arrow passes through a non-plausible solution, the convex boundary is less curved than the concave boundary, hence the gap cannot be closed without the curves touching elsewhere (near the actual contact candidates in blue). If the boundaries do not overlap, then plausible contact candidates are local minimizers of the distance. If there are overlaps, then plausible pairs are local maximizers of the penetration between the bodies.

Intersection points ($\Gamma_A = \Gamma_B$) are also possible solutions of eq. (2). This type of solution, however, is also disregarded, because, among other reasons, the definition of the contact normal direction is not straightforward at an intersection in general.

3 Hertzian formulae for two-dimensional contact

For two cylindrical bodies made of linear elastic materials with their axes aligned, we have the following results: the distribution of pressure is semi-elliptical (simply referred to as elliptical onward)

$$p(x) = p_0 \left(1 - \frac{x^2}{a^2}\right)^{1/2}, \tag{3}$$

with the maximum pressure

$$p_0 = \frac{2P}{\pi a}, \tag{4}$$

the length a is half the size of the contact patch, which is related to the load per unit length P by

$$a^2 = \frac{4PR}{\pi E^*}, \tag{5}$$

where E^* is the equivalent Young modulus

$$\frac{1}{E^*} = \frac{1-\nu_1^2}{E_1} + \frac{1-\nu_2^2}{E_2}, \tag{6}$$

and R is the relative radius of curvature at the contact pair

$$\frac{1}{R} = \frac{1}{R_1} + \frac{1}{R_2}. \tag{7}$$

The elastic properties of body i are its Young Modulus E_i and Poisson ratio ν_i, R_i is the curvature radius at the contact point of body i, for a concave boundary, the radius is negative.

Unlike in three dimensions, it is not possible to define a universal relation between indentation and load $P(\delta)$ only considering elastic half-space models for the bodies, the relation depends on their whole geometries and boundary conditions [3].

4 Description of the problem

In this work, we will analyze the two-dimensional contact of a convex particle with a concavity. Using the software Abaqus® [6], we create and solve a finite element model, from which we obtain the pressure distribution over the concave surface. The main goal of the present work is to investigate the effects of the deformations on the surface pressure distribution and compare it with the Hertz solution.

The smooth contact boundaries are cubic B-splines modeled in the software Abaqus®. Copies of the undeformed curves are used to keep track of the contact pairs found solving eq. (2). The convex curve was closed with a circular arc tangent to both ends. The concave body was closed using line segments, two vertical lines for the sides, one horizontal line for the bottom. The convex body is perfectly rigid and the concave body is made of a hypothetical linear elastic material with properties $E = 214$ GPa and $\nu = 0.3$. The equivalent stifness of the pair is $E^* = 235$ GPa. No plasticity is considered. The contact interaction is frictionless. A surface-to-surface discretization method was used with the rigid boundary as the master surface and the concave boundary as the slave surface.

The bottom line and the sides of the deformable body are fully constrained, while the contact surface is free to move. The constrained lines are far from the contact region to diminish the effects of the boundary conditions on the contact pressure. The only present loads are prescribed displacements of the convex particle, which is initially positioned in two special configurations with gaps to the concave body and known solutions of the LCP (see Fig. 2). The first initial configuration is symmetrical with two far-apart solutions. The second is a “close-to-conformal” configuration with two near contact candidates. From each initial position, the convex particle is translated by static steps along the lines indicated in Fig. 2 by the red arrows, the maximum displacement is 1 mm.

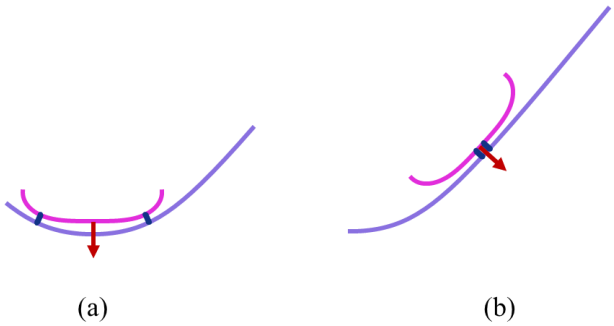

Figure 2. Contact surfaces and initial configurations (a) symmetrical, and (b) close-to-conformal

5 Results

The finite element analysis (FEA) results in the pressure distribution (in MPa) over the concave boundary for multiple configurations of the convex particle. The pressure is given in function of an arc-length parameter of the undeformed concave boundary (the lengths are measured in milimeters). The integration of the pressure results in the load per longitudinal length P (given in N/mm). The maximum pressure p_0 is also available. Table 1 summarizes the numerical values related to the contact patches for different configurations, indexed by the displacement d (in mm). The indentation δ is the distance between the points represented by a plausible solution of eq. (2).

Table 1. Properties of the contact patches

Configuration	d (mm)	δ (mm)	P (N/mm)	p_0 (MPa)
Symmetrical	0.60	0.086	5106	8361
	0.80	0.27	17693	15444
	1.00	0.46	31393	20620
Close-to-conformal	0.46	0.00043	208	578
	0.47	0.010	979	1143
	0.48	0.020	1862	1518
	0.50	0.040	3688	2179
	0.70	0.24	23560	7569
	1.00	0.54	55625	13879

Figure 3 represents the relations between the total load and the indentation in the two cases. It shows that the close-to-conformal contact is stiffer, a property expected of a conformal contact, which spreads the load over a larger area.

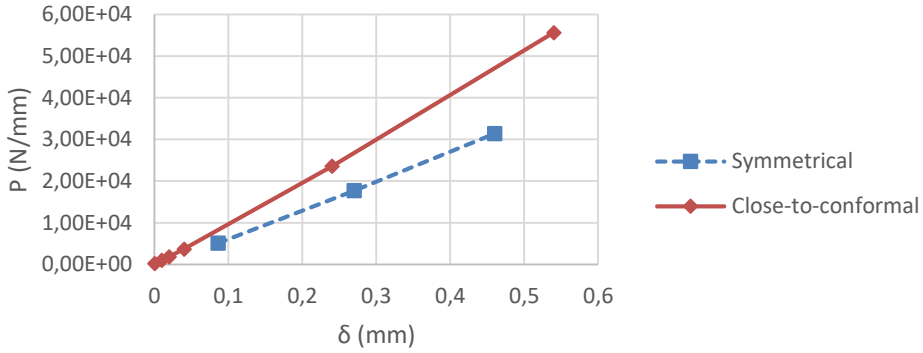

Figure 3. Total load versus indentation

5.1 Symmetrical configurations

In the first case, non-conformal contact occurs in two regions that are symmetricaly distributed. Figure 4 presents the distribution of pressure for one of the contact patches with incresing values of indentation. For the indentation $\delta = 0.086$ mm, corresponding to the prescribed displacement $d = 0.60$ mm, the pressure is well approximated by an ellptical distribution. Using eq. (4), we calculate the equivalent contact patch size of an elliptical distribution of pressure with the same maximum value and integral, which is 0.78 mm. The elliptical distribution is fitted to the FEA result in order to compare them. The comparison is based on the root mean square (RMS) of the difference between the distributions. The ratio of the RMS and the maximum pressure in this case is 7.49×10^{-3}, which means the RMS is negligible in comparison with the maximum pressure.

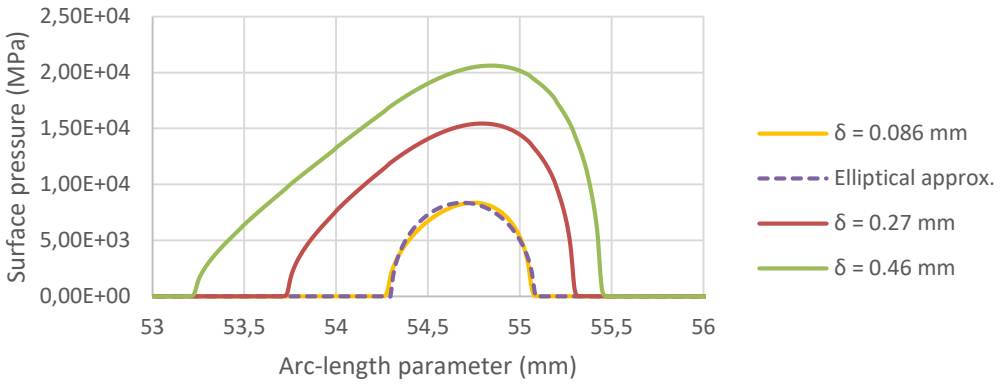

Figure 4. Pressure distributions over the right contact patch of the symmetrical configuration for different values of indentation

Solving the LCP for the rigid boundaries, we get the two symmetrical contact pairs. Still considering $\delta = 0.086$ mm, the curvature radii are 2.96 mm and 6.81 mm for the convex and the concave boundary respectively. Thus, the relative radius is 5.23 mm. Equation (5), then, yields the size of the contact patch as 0.76 mm, reasonably close to the value obtained with eq. (4). Therefore, we can say the two simultaneous contacts are Hertzian and independent.

The other plots in Fig. 4 show that the pressure becomes noticeably non-elliptical for larger displacements. The contacts are not Hertzian anymore because they start to interfere with each other via the stress/strain field in the concave body, as one can see in Fig. 5.

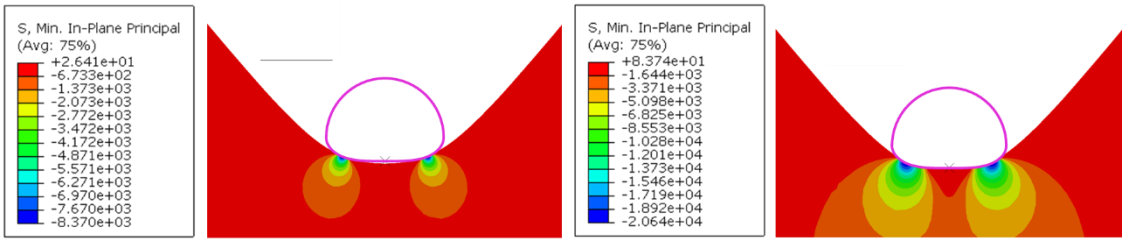

Figure 5. Minimum principal stress field in the concave body for the symmetrical configurations

5.2 Close-to-conformal contact

The second group of configurations is the close-to-conformal, referred this way because the LCP has two very close solutions that, presumably, interfere even for small deformations. Figure 6 shows the numerical results for three displacements approaching the value $d = 0.50$ mm, corresponding to the indentations indicated. For the

smallest indentation (obtained for $d = 0.46$ mm), it is possible to fit an elliptical distribution to the FEA result. The equivalent contact patch has a size 0.46 mm according to eq. (4). The ratio of the RMS and the maximum pressure in this case is 5.00×10^{-3}, it is a better fit than the one shown in Fig. 4. The primary solution of the LCP represents a pair of points with radii 41 mm (convex) and 50 mm (concave), which results in a relative radius 233 mm, a large relative radius is another indication of conformal contact. Equation (5) yields the size of the contact patch as 1.02 mm. There is no agreement between the results of eq. (4) and eq. (5) by considering the traditional solution of the LCP.

After further inspection, we noticed that the leftmost intersection of the curves occurs at points with radii 23 mm (convex) and 44 mm (concave), which results in a relative radius 50 mm. Considering the intersection point, the patch size computed from eq. (5) is 0.47 mm, which agrees with eq. (4). Therefore, the contact is indeed Hertzian, but the actual contact pair is not as expected.

The intermediate indentation represents the effects of the activation of the secondary contact pair. As we can see, there are two contact patches separated by a short distance. The elliptical aspect of the pressure distribution is lost due to their intereference.

Finally, for the largest indentation, the pressure distributions merge. The surface pressure becomes clearly non-elliptical, and differs from a superposition of two elliptical distributions. The superposition of supposedly independent pressure distributions is not a good strategy when dealing with close-to-conformal configurations.

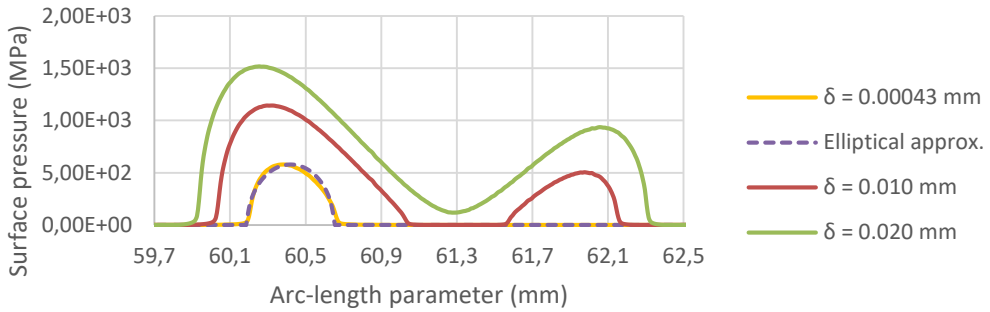

Figure 6. Pressure distributions over the contact patch of the close-to-conformal configuration for three levels of displacement: (1) primary contact pair activated, (2) secondary contact pair activated, and (3) contact patches merged

Figure 7 shows the effect of further increasing the indentation ($\delta = 0.54$ mm corresponds to the displacement 1 mm). The minimum principal stress fields are shown in Fig. 8 for the configuration representing the appearance of the secondary contact and the configuration corresponding to the largest load respectivelly.

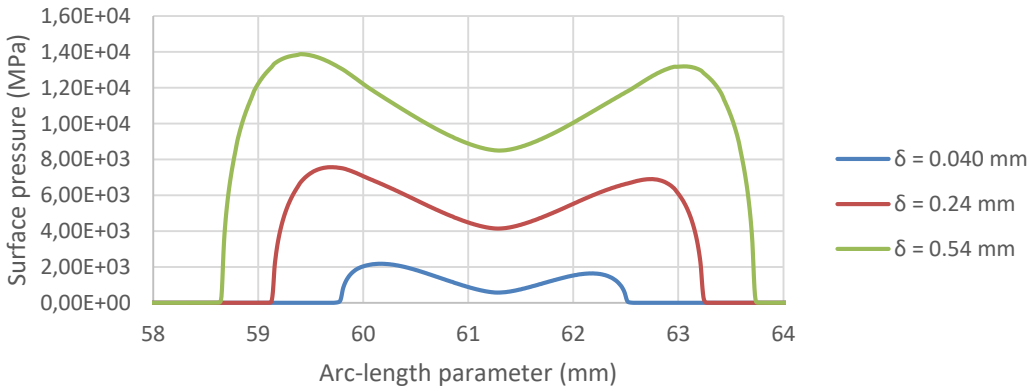

Figure 7. Pressure distributions over the contact patch of the close-to-conformal configuration for larger displacements/indentations

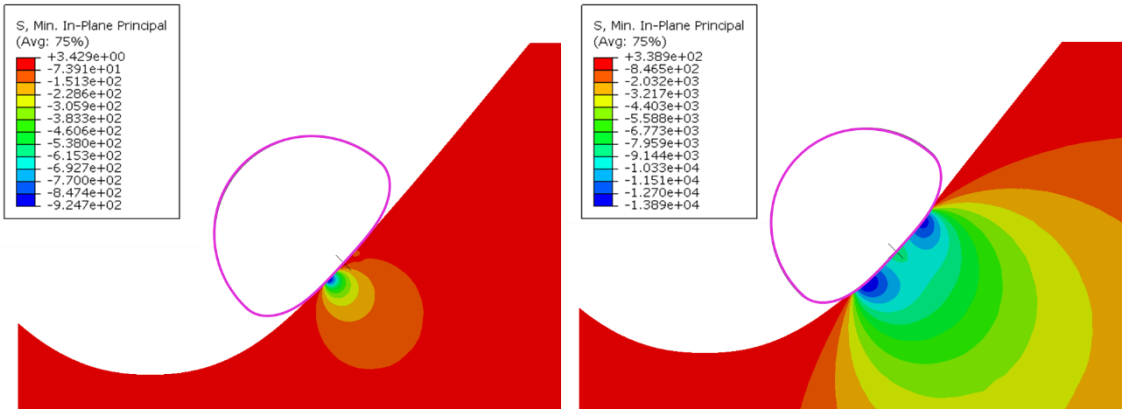

Figure 8. Minimum principal stress field in the concave body for the close-to-conformal configurations

6 Conclusions

Using a numerical model we explored some limits of the Hertz contact theory. In a non-convex contact, multiple contact points may be present, one must be careful that they are sufficiently far apart to not interfere with each other. Distant contact points may be treated as independent Hertzian contacts. On the other hand, very close contact points may interfere even when the deformation is small, making a non-Hertzian contact patch. Superposition of the independent pressure distributions does not give satisfactory results in this case.

Acknowledgements. This work was financed in part by the Coordenação de Aperfeiçoamento de Pessoal de Nível Superior - Brasil (CAPES) - Finance Code 001, and supported by Vale S.A. through the Wheel-Rail Chair project. The second author acknowledges CNPq (Conselho Nacional de Desenvolvimento Científico e Tecnológico) for the financial support under the research grant 304321/2021-4.

Authorship statement. The authors hereby confirm that they are the sole liable persons responsible for the authorship of this work, and that all material that has been herein included as part of the present paper is either the property (and authorship) of the authors, or has the permission of the owners to be included here.

References

[1] A. Gay Neto, "Framework for automatic contact detection in a multibody system". *Computer Methods in Applied Mechanics and Engineering*, vol. 403, 2023.
[2] L. da Silva and A. Gay Neto, "Contact interaction law based on the Hertz theory for multibody applications". In: XLIII CILAMCE, 2022.
[3] K. L. Johnson. *Contact mechanics*. Cambridge University Press, 1985.
[4] E. E. Magel and J. Kalousek. "The application of contact mechanics to rail profile design and rail grinding". *Wear*, vol. 253, n. 1, pp. 308-316, 2002.
[5] A. Gay Neto and P. Wriggers. "Numerical method for solution of pointwise contact between surfaces". *Computer Methods in Applied Mechanics and Engineering*, vol. 365, 2020.
[6] Dassault Systèmes. "Abaqus Analysis User's Guide". *Dassault Systèmes*, 2016. [Online]. Available: http://130.149.89.49:2080/v2016/books/usb/default.htm.